STABILITY OF INTERPLAY MOTIONS

M. HÉNON

Observatoire de Nice, France

(Received 17 February, 1976)

Abstract. A family of rectilinear periodic solutions of the three-body problem, in which the central body collides alternately with each of the two other bodies, is investigated numerically for all values of the three masses. It is found that for every mass combination there exists just one solution of this kind. The linear stability of the orbits with respect to arbitrary three-dimensional perturbations is also investigated. Domains of stability and instability are displayed in a triangular mass diagram. Their boundaries form one-parameter families of critical orbits, which are tabulated. Limiting cases where one or two masses vanish are studied in detail. The domains of stability cover nearly one half of the total area in the mass diagram: this reinforces the conclusion that real triple stars might have motions of a kind entirely different from the usual hierarchical arrangement.

1. Introduction

In a previous paper (Hénon, 1976), it was unexpectedly found that a rectilinear periodic solution of the three-body problem originally computed by Schubart (1956) was linearly stable in three-dimensional space. Moreover, this particular orbit was the origin of a family of plane periodic solutions, and along this family a sizeable interval was found where the orbits retained two-dimensional stability. These orbits were of the 'interplay' type (Szebehely, 1971), with alternating close approaches of body 2 with bodies 1 and 3. This indicated the possible existence of triple stars with a motion radically different from the usual hierarchical arrangement.

These results were limited to the particular case of three equal masses, and it would be of interest to explore more generally the stability of interplay orbits for all possible values of the three masses. But a given mass combination is represented essentially by 2 parameters (the total mass can be normalized to 1); and for given masses, there exists a one-parameter family of periodic orbits. Thus, a full exploration would require the computation of a 3-parameter set of periodic orbits and of their stability, and would represent a considerable amount of work.

We settle therefore for a more modest objective: we let the masses have all possible values, but for given masses we consider only one particular member of the one-parameter family of periodic orbits. Thus we deal only with a 2-parameter set of periodic orbits, which proves to be manageable. The particular member which we select is simply the rectilinear periodic orbit (as we shall see, this orbit continues to exist when the masses are varied). Such a choice may seem paradoxical since this particular orbit is completely unrealistic: it cannot exist in real systems because of the collisions. On second thought, however, this choice offers a number of advantages. First of all, the rectilinear orbit is the only one for which a determination of the linear

Celestial Mechanics **15** (1977) 243–261.

stability in the plane suffices to determine also the three-dimensional stability; this is a consequence of the axial symmetry (Hénon, 1976). Second, if for some given values of the masses the three stability indices of the rectilinear orbit are found to satisfy

$$|k_i| < 2, \qquad (i = 1, 2, 3), \tag{1}$$

then there will be a finite interval along the family of plane orbits for which (1) is still satisfied. In other words, there will exist not only a stable rectilinear orbit but also stable interplay orbits, free of collisions and therefore representing possible motions of real systems. Third, the rectilinear orbits represent a particular case of the three-body problem which is of interest in itself; and finally, they are particularly easy to compute because of their simplicity. The collisions are no problem when an adequate regularization is used (see Hénon, 1974).

2. Results

We consider periodic rectilinear solutions carried by the x axis; the system is then defined by the masses m_i, the positions x_i and the velocities $\dot{x}_i = u_i$ $(i = 1, 2, 3)$. We number the bodies in order of increasing abscissas:

$$x_1 \leqslant x_2 \leqslant x_3; \tag{2}$$

this order is invariant in time. We use the normalization described in a previous paper (Hénon, 1974). The gravitational constant is equal to 1. The sum of the three masses is normalized to 1:

$$m_1 + m_2 + m_3 = 1. \tag{3}$$

The origin is the center of mass of the system:

$$m_1 x_1 + m_2 x_2 + m_3 x_3 = 0, \qquad m_1 u_1 + m_2 u_2 + m_3 u_3 = 0. \tag{4}$$

The dimensions are scaled in such a way that the total energy is

$$E = \tfrac{1}{2}(m_1 u_1^2 + m_2 u_2^2 + m_3 u_3^2) - \frac{m_2 m_3}{x_3 - x_2} - \frac{m_3 m_1}{x_3 - x_1} - \frac{m_1 m_2}{x_2 - x_1} =$$

$$= -\tfrac{1}{2}(m_2 m_3 + m_3 m_1 + m_1 m_2). \tag{5}$$

Finally, the origin of time is defined by the condition

$$u_1 = u_3. \tag{6}$$

A given mass combination can be conveniently represented by a point in a triangular mass diagram (Figure 1): the distances of the point to the three sides represent the three masses. The height of the triangle must then equal 1 to satisfy (3). Similar mass diagrams have been used before by Szebehely (1972) and Standish (1972).

For given masses, the rectilinear three-body problem has in general isolated periodic solutions; if the masses are allowed to vary, each of these solutions generates

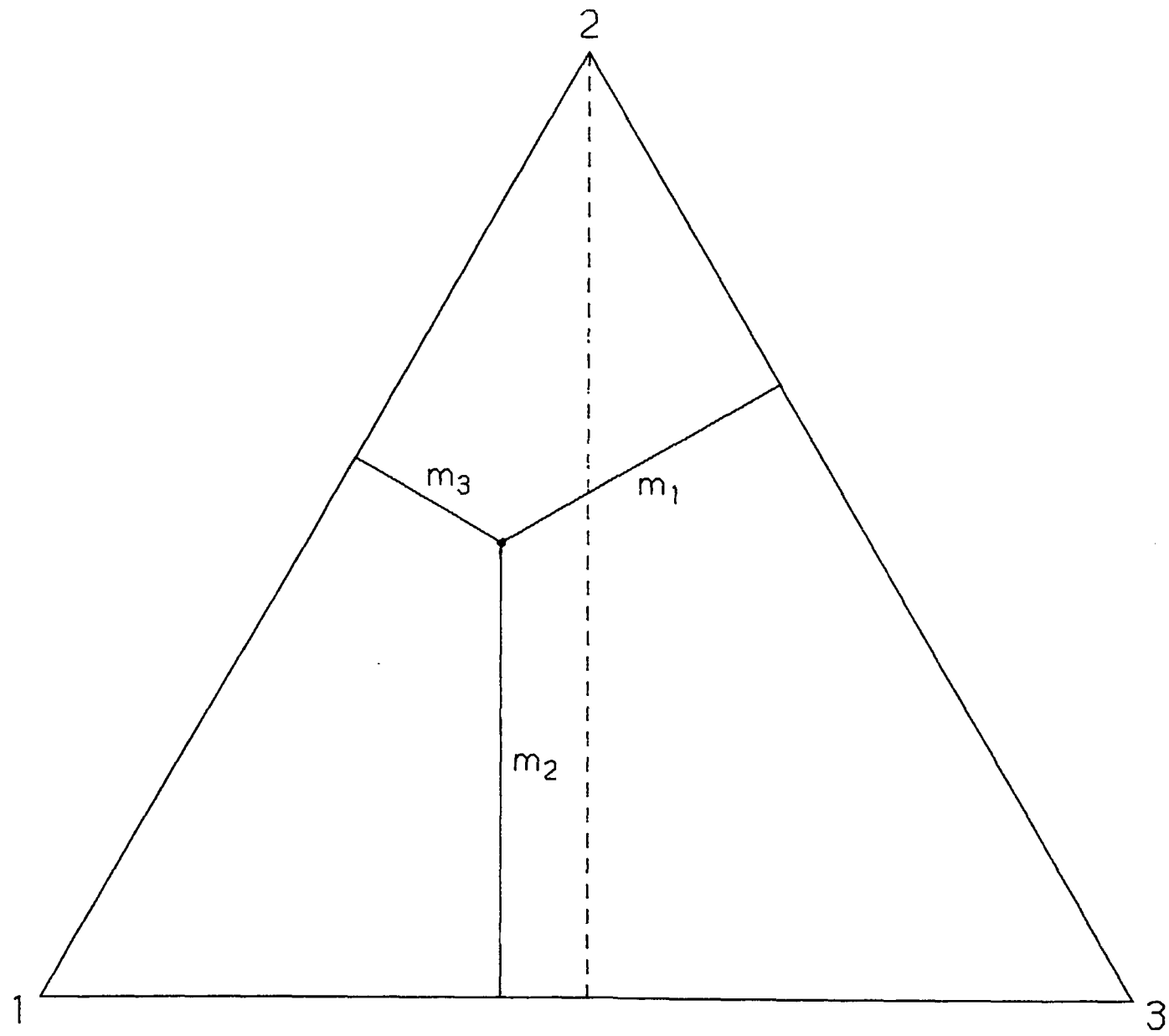

Fig. 1. The mass diagram.

a two-parameter family of periodic solutions (Hénon, 1974). Here we start from Schubart's orbit, an isolated solution for the case $m_1=m_2=m_3$, and we consider the two-parameter family generated by it when the masses are varied. Schubart's orbit is represented by a point at the center of the triangle in Figure 1; and locally at least, there should be a one-to-one correspondence between the members of the two-parameter family and the representative points in Figure 1. This is confirmed by the numerical computations. Moreover, the one-to-one correspondence turns out to exist not only in the neighborhood of the center, but throughout the triangle: for every mass combination, there exists exactly one member of the family. In other words, this family, considered as a function of two variables, has a single sheet which covers the whole triangle. (It can even be extended beyond the border of the triangle, but this is of no astronomical interest since one or two of the masses are then negative.)

A typical solution is shown on Figure 2; it corresponds to the point shown on Figure 1, and to the particular values $m_1=0.34$, $m_2=0.48$, $m_3=0.18$. The positions of the three bodies on the x axis are represented as functions of time. The period is $T=5.485\,617\ldots$; two full periods are represented. The motion is symmetrical with respect to the time t_0 of a collision 1–2:

$$x_i(t_0+\tau)=x_i(t_0-\tau), \qquad u_i(t_0+\tau)=-u_i(t_0-\tau). \tag{7}$$

It is also symmetrical with respect to the time $t_0+T/2$ of a collision 2–3. In view of these symmetries, it might have been more logical to define the origin of time as the time of a collision; however, this would raise practical problems because two velocities

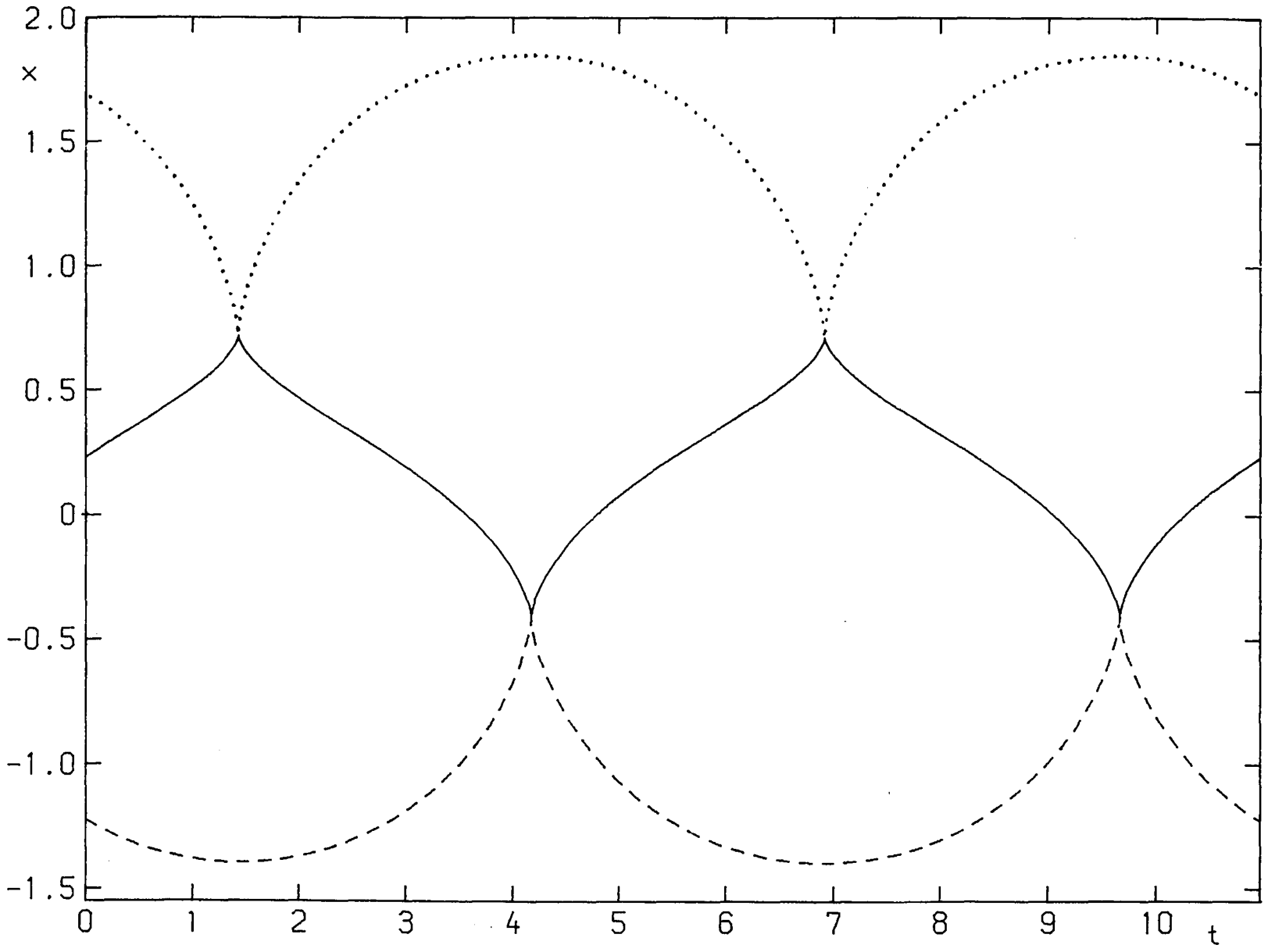

Fig. 2. Positions of the three bodies as functions of time, for a typical rectilinear orbit.

are then infinite and the initial conditions can only be specified in regularized variables. By contrast, the convention (6) ensures that the computation begins and ends away from collisions.

We turn now to the linear stability of the orbits. It will depend on the values of two stability indices, k_1 and k_2, which are related respectively to longitudinal and transversal perturbations (see Hénon, 1976, where the practical procedure for computing k_1 and k_2 is also given). These indices are always real. They change continuously as the representative point moves in the mass diagram of Figure 1, and our problem is to find the regions where the two following inequalities are simultaneously satisfied:

$$|k_1| < 2, \qquad |k_2| < 2; \tag{8}$$

these will be the regions of three-dimensional stability.

To this end, the triangle of Figure 1 was explored along a number of vertical 'sections'. Each section is thus characterized by a constant value of $m_1 - m_3$, and m_2 is used as a parameter. There is a symmetry in the problem: two points which are symmetrical with respect to the vertical axis (dashed line on Figure 1) represent essentially the same orbit, with only the direction of the x axis inverted and the names of bodies 1 and 3 exchanged. This symmetry is apparent in the results (Figure 5 below). Therefore it is sufficient to explore the left half of the triangle, corresponding to $m_1 \geqslant m_3$.

In each section, the stability indices were computed for a number of orbits, and then plotted as a function of m_2. Figure 3 shows typical results for the section

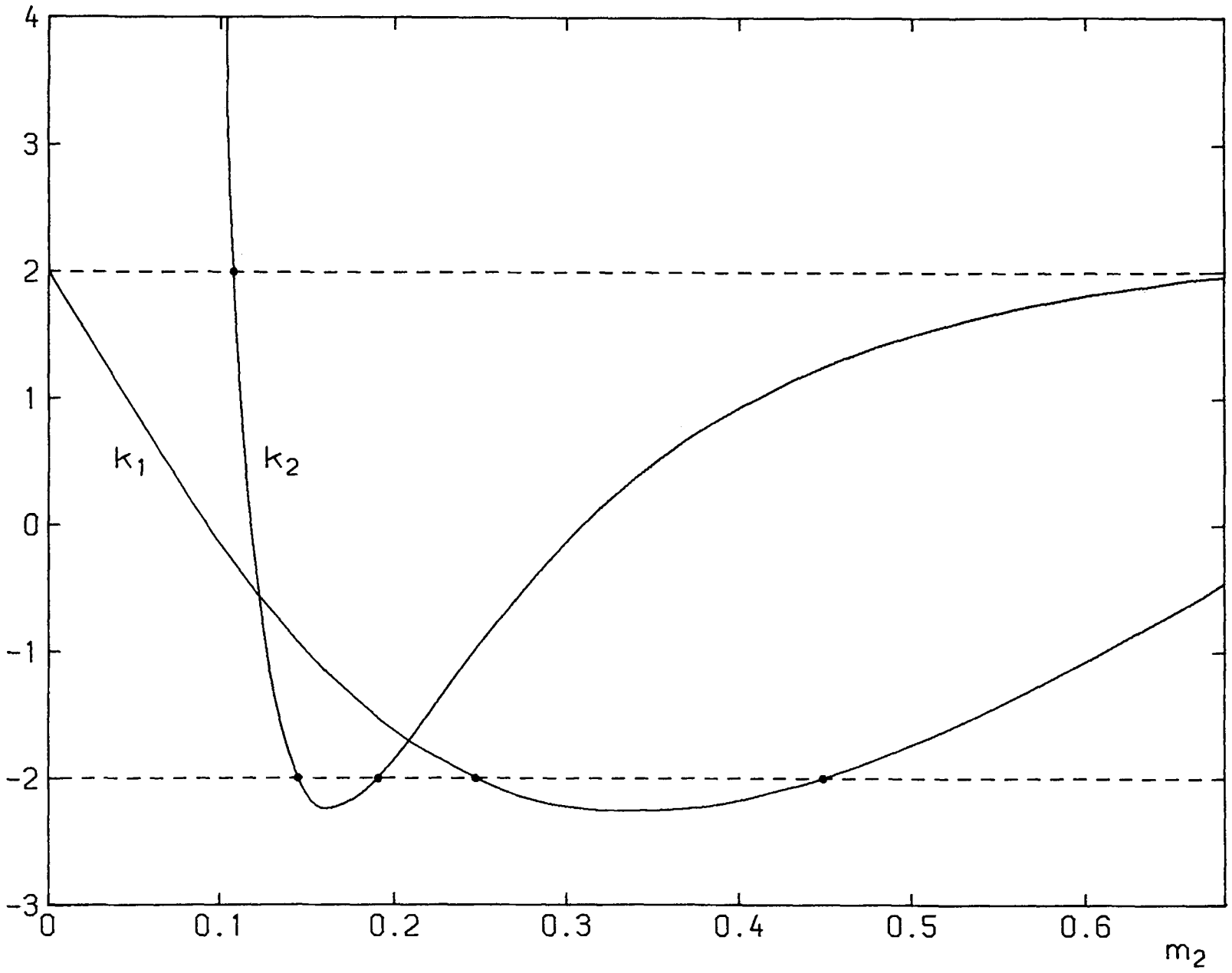

Fig. 3. Stability indices k_1 and k_2 along a section of the mass diagram defined by $m_1 - m_3 = 0.32$.

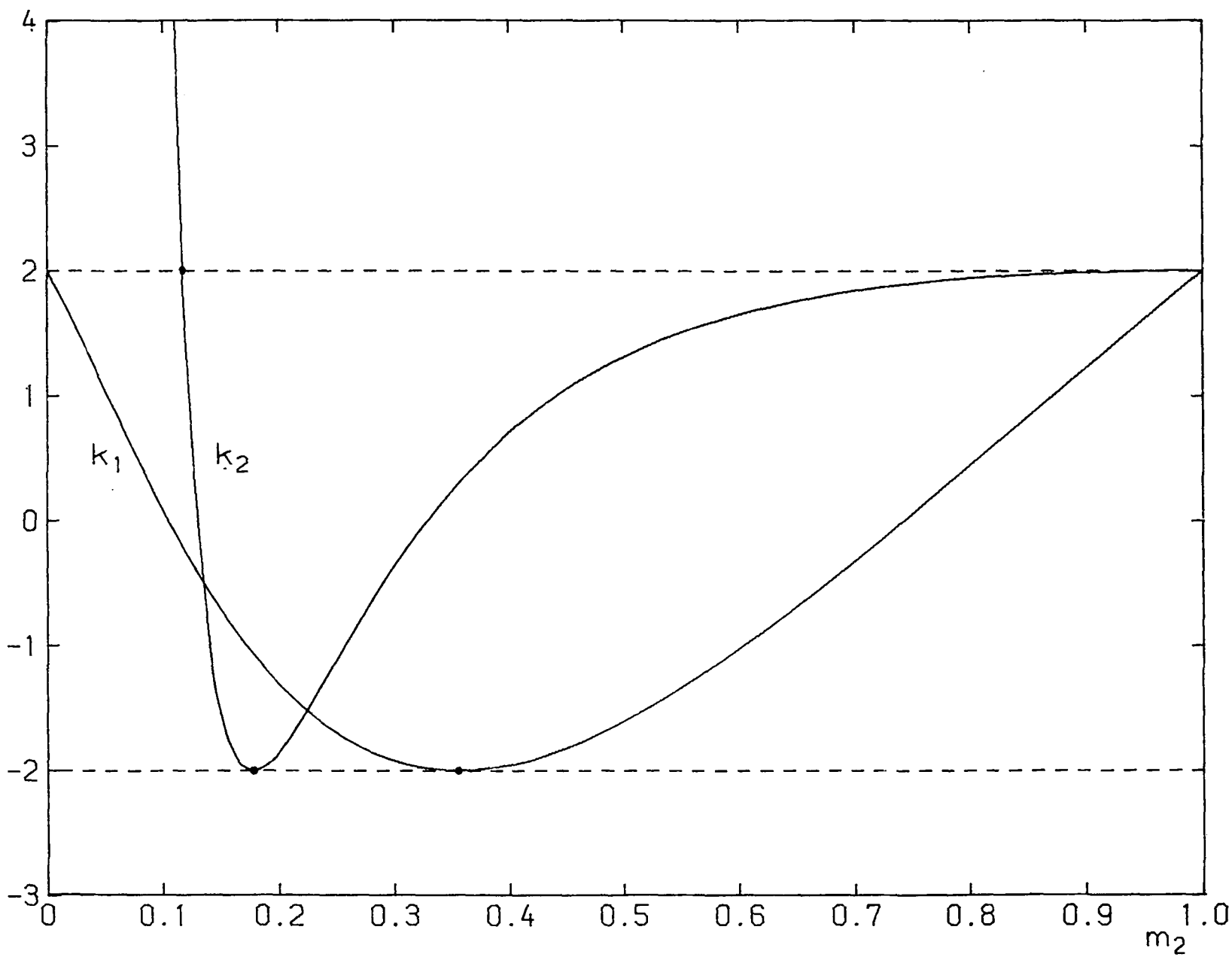

Fig. 4. Stability indices k_1 and k_2 along a section of the mass diagram defined by $m_1 - m_3 = 0$.

$m_1 - m_3 = 0.32$. Critical orbits, corresponding to $|k_1| = 2$, or $|k_2| = 2$, were computed by an iterative process; they are represented by dots on Figure 3. Along this particular section, one thus finds that the orbits are longitudinally unstable for $0.246\,958... < m_2 < 0.448\,362...$; they are transversally unstable for $m_2 < 0.107\,484...$ and for $0.144\,496 < m_2 < 0.190\,550....$

The section $m_1 - m_3 = 0$ (dashed line in Figure 1) is of particular interest since it corresponds to a symmetrical mass configuration. It is represented on Figure 4. The curves $k_1(m_2)$ and $k_2(m_2)$ touch the line $k_i = -2$, at $m_2 = 0.354\,838...$ and $m_2 = 0.178\,072...$ respectively. This peculiarity is a consequence of the symmetry and can be explained as follows. Consider a particular orbit with $m_1 = m_3$, with period T. If, after one half-period, we invert the direction of the x axis and exchange bodies 1 and 3, we find that the initial configuration is recovered. In other words, in this special case the orbit can be considered as having a period $T/2$. This shorter periodic orbit has two stability indices, which we call k_1' and k_2'. Let λ_{i1}' and λ_{i2}' be the two eigenvalues associated with k_i'; there is

$$\lambda_{i1}' + \lambda_{i2}' = k_i', \qquad \lambda_{i1}'\lambda_{i2}' = 1. \tag{9}$$

The eigenvalues for the full periodic orbit of period T are

$$\lambda_{i1} = \lambda_{i1}'^2, \qquad \lambda_{i2} = \lambda_{i2}'^2, \tag{10}$$

and we have

$$k_i = \lambda_{i1} + \lambda_{i2} = k_i'^2 - 2. \tag{11}$$

This immediately shows that $k_i \geqslant -2$, and that k_i will touch the value -2 whenever k_i' changes sign. A similar effect operates in the circular restricted problem when the masses of the primaries are equal (Hénon, 1973).

With the help of a number of sections similar to Figures 3 and 4, the domains of stability and instability were mapped in the mass diagram. Figure 5 shows the result. Horizontally hatched regions correspond to longitudinal instability, i.e. $|k_1| > 2$; vertically hatched regions correspond to transversal instability, i.e., $|k_2| > 2$. Therefore the orbits are three-dimensionally stable in the white regions, and unstable in all hatched regions.

We see thus that the stability of the rectilinear orbit, established in our earlier paper for the case of three equal masses, exists also for many other mass combinations, though not for all. The regions of stability represent about 46% of the total area of the triangle. This reinforces the conclusion that real triple stars might have an interplay type of motion, entirely different from the classical hierarchical configuration which until now was generally believed to be the only stable arrangement for stars of comparable masses.

The three regions of stability in Figure 5 have a somewhat complex shape, and cannot be characterized in a few words. Very roughly, however, it can be said that stability tends to prevail when the central mass m_2 increases. In particular, the largest stability

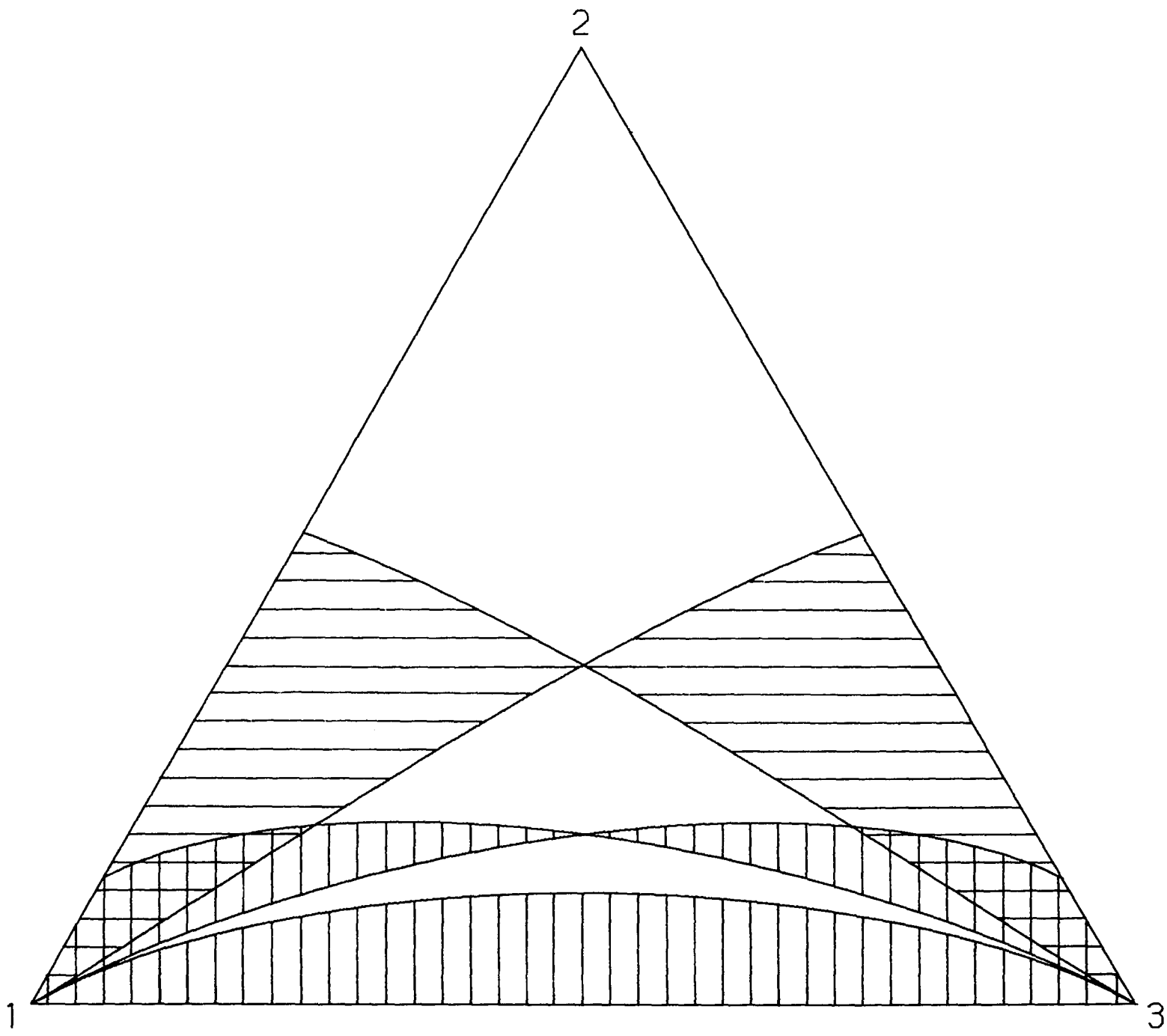

Fig. 5. Domains of stability (white), longitudinal instability (horizontal hatching), transversal instability (vertical hatching) in the mass diagram.

region, at the top of the triangle in Figure 5, happens to be represented in good approximation by

$$m_2 > m_1 \quad \text{and} \; m_2 > m_3, \tag{12}$$

i.e., the central mass is the largest of the three. That such configurations are stable is intuitively natural. But there are also stable mass configurations in which the central mass is not the largest, as shown by the two lower white regions in Figure 5.

The boundaries of the regions correspond to one-parameter families of critical periodic orbits. These families are given by Tables I to III. Each critical orbit was determined with an accuracy of the order of 10^{-8}. Only one half of the boundaries is given; the other half is deduced by symmetry, i.e. exchanging m_1 and m_3, x_1 and x_3. To save space, only the initial coordinates x_1, x_3, $u_1 = u_3$ are listed; the initial values of x_2 and u_2 can be deduced from (4). Our program uses Waldvogel's regularization (1972), which requires that all three masses be finite; this probably explains our finding that the numerical accuracy deteriorates when one of the masses becomes very small. As a consequence, the limiting cases in which one or two masses vanish could not be computed directly. The initial lines of Tables I to III, corresponding to $m_2 = m_3 = 0$, were derived from an analysis of the limit (see below Section 3); the last lines of

TABLE I

Critical periodic orbits, $k_1 = -2$

m_1	m_2	m_3	x_1	x_3	$u_1 = u_3$	T	k_2
1.	0.	0.	0.	2.	0.	3.141 593	∞
0.973 090	0.013 820	0.013 090	−0.032 558	2.046 487	−0.027 931	3.299 608	−16.235 7
0.918 727	0.042 546	0.038 727	−0.111 213	2.050 788	−0.059 544	3.477 898	−8.964 711
0.864 066	0.071 868	0.064 066	−0.200 214	2.023 908	−0.082 935	3.617 523	−6.153 751
0.809 295	0.101 410	0.089 295	−0.296 196	1.981 592	−0.102 294	3.741 601	−4.517 760
0.754 513	0.130 974	0.114 513	−0.397 469	1.929 414	−0.119 178	3.857 917	−3.406 928
0.699 792	0.160 416	0.139 792	−0.503 085	1.870 178	−0.134 383	3.970 494	−2.585 521
0.650 504	0.186 790	0.162 706	−0.601 686	1.812 034	−0.147 039	4.071 066	−2.
0.645 188	0.189 624	0.165 188	−0.612 511	1.805 526	−0.148 356	4.081 937	−1.943 396
0.590 750	0.218 500	0.190 750	−0.725 477	1.736 509	−0.161 366	4.194 224	−1.420 913
0.536 521	0.246 958	0.216 521	−0.841 898	1.663 848	−0.173 576	4.309 069	−0.982 418
0.482 546	0.274 908	0.242 546	−0.961 830	1.588 060	−0.185 086	4.428 123	−0.604 976
0.428 867	0.302 266	0.268 867	−1.085 466	1.509 528	−0.195 951	4.553 129	−0.272 955
0.375 530	0.328 940	0.295 530	−1.213 134	1.428 544	−0.206 197	4.686 046	0.024 857
0.322 581	0.354 838	0.322 581	−1.345 328	1.345 328	−0.215 824	4.829 213	0.296 891
0.270 074	0.379 852	0.350 074	−1.482 746	1.260 051	−0.224 812	4.985 537	0.549 805
0.218 066	0.403 868	0.378 066	−1.626 365	1.172 831	−0.233 117	5.158 782	0.789 158
0.166 622	0.426 756	0.406 622	−1.777 553	1.083 744	−0.240 673	5.353 989	1.019 893
0.115 819	0.448 362	0.435 819	−1.938 264	0.992 816	−0.247 381	5.578 160	1.246 752
0.065 747	0.468 506	0.465 747	−2.111 349	0.900 008	−0.253 102	5.841 407	1.474 677
0.016 515	0.486 970	0.496 515	−2.301 111	0.805 200	−0.257 640	6.158 982	1.709 301
0.	0.492 82	0.507 18	−2.370 49	0.772 48	−0.258 87	6.283 185	1.791 74

Tables I and II, corresponding to $m_1 = 0$, were obtained by interpolation from neighboring values and are therefore somewhat less accurate.

Figure 5 shows that the boundary lines corresponding respectively to $k_1 = -2$ and $k_2 = -2$ intersect at two symmetrical points. These points represent a *doubly critical orbit*. The values of the masses are (for the point at the left):

$$m_1 = 0.650\,504\ldots, \qquad m_2 = 0.186\,790\ldots, \qquad m_3 = 0.162\,706\ldots. \tag{13}$$

Table IV lists the family of ordinary periodic orbits for the symmetrical case, $m_1 = m_3$ (see Figure 4). Again the first and last lines were derived from an analysis of the limiting cases (Section 3).

3. Limiting Cases

The sides and the vertices of the triangle (Figures 1 and 5) correspond to cases where one or two masses vanish, and are of particular interest. Because of the symmetry, only four cases need be distinguished; we shall examine them in turn.

(a) *Limit* $m_3 \to 0$. This corresponds to the left side of the triangle. In this limit we obtain the rectilinear restricted problem of three bodies. The primaries are bodies 1 and 2, which describe an elliptical two-body orbit with eccentricity 1. Taking into

TABLE II

Critical periodic orbits, $k_2 = -2$

m_1	m_2	m_3	x_1	x_3	$u_1 = u_3$	T	k_1
1.	0.	0.	0.	2.	0.	3.141 593	−2.
0.973 707	0.012 586	0.013 707	−0.032 258	1.988 976	−0.026 571	3.091 259	−1.631 0
0.922 389	0.035 222	0.042 389	−0.106 710	1.934 263	−0.054 242	3.056 634	−1.340 192
0.872 234	0.055 532	0.072 234	−0.186 984	1.868 825	−0.073 353	3.044 225	−1.179 305
0.823 004	0.073 992	0.103 004	−0.270 573	1.798 746	−0.088 201	3.043 438	−1.075 164
0.774 577	0.090 846	0.134 577	−0.356 474	1.726 033	−0.100 305	3.050 991	−1.005 294
0.726 879	0.106 242	0.166 879	−0.444 218	1.651 615	−0.110 429	3.065 472	−0.959 567
0.679 861	0.120 278	0.199 861	−0.533 593	1.575 986	−0.119 014	3.086 252	−0.932 656
0.633 493	0.133 014	0.233 493	−0.624 534	1.499 425	−0.126 337	3.113 132	−0.921 596
0.587 752	0.144 496	0.267 752	−0.717 071	1.422 099	−0.132 581	3.146 198	−0.924 779
0.542 629	0.154 742	0.302 629	−0.811 314	1.344 099	−0.137 867	3.185 773	−0.941 505
0.498 119	0.163 762	0.338 119	−0.907 437	1.265 475	−0.142 276	3.232 405	−0.971 771
0.454 227	0.171 546	0.374 227	−1.005 684	1.186 240	−0.145 858	3.286 886	−1.016 200
0.410 964	0.178 072	0.410 964	−1.106 380	1.106 380	−0.148 639	3.350 303	−1.076 066
0.368 349	0.183 302	0.448 349	−1.209 948	1.025 859	−0.150 625	3.424 120	−1.153 398
0.326 409	0.187 182	0.486 409	−1.316 944	0.944 616	−0.151 804	3.510 304	−1.251 204
0.285 183	0.189 634	0.525 183	−1.428 102	0.862 562	−0.152 141	3.611 539	−1.373 846
0.244 725	0.190 550	0.564 725	−1.544 417	0.779 577	−0.151 579	3.731 550	−1.527 679
0.205 105	0.189 790	0.605 105	−1.667 273	0.695 496	−0.150 030	3.875 662	−1.722 168
0.166 422	0.187 156	0.646 422	−1.798 668	0.610 092	−0.147 365	4.051 778	−1.971 921
0.162 706	0.186 790	0.650 504	−1.812 034	0.601 686	−0.147 039	4.071 066	−2.
0.128 814	0.182 372	0.688 814	−1.941 626	0.523 048	−0.143 393	4.272 220	−2.300 666
0.092 483	0.175 034	0.732 483	−2.101 022	0.433 895	−0.137 824	4.557 517	−2.749 765
0.057 747	0.164 506	0.777 747	−2.285 446	0.341 909	−0.130 188	4.945 191	−3.398 939
0.025 154	0.149 692	0.825 154	−2.512 146	0.245 850	−0.119 654	5.513 957	−4.426 875
0.	0.132 1	0.867 9	−2.768 5	0.159 4	−0.107 2	6.283 185	−5.963 3

TABLE III

Critical periodic orbits, $k_2 = +2$

m_1	m_2	m_3	x_1	x_3	$u_1 = u_3$	T	k_1
1.	0.	0.	0.	2.	0.	3.141 593	−2.
0.973 836	0.012 328	0.013 836	−0.032 187	1.976 450	−0.026 277	3.046 373	−1.552 7
0.923 433	0.033 134	0.043 433	−0.105 295	1.898 245	−0.052 629	2.929 132	−1.144 490
0.874 856	0.050 288	0.074 856	−0.182 230	1.812 633	−0.069 987	2.842 206	−0.893 368
0.827 684	0.064 632	0.107 684	−0.260 541	1.725 637	−0.082 862	2.773 279	−0.715 186
0.781 661	0.076 678	0.141 661	−0.339 388	1.638 897	−0.092 859	2.717 500	−0.581 642
0.736 614	0.086 772	0.176 614	−0.418 440	1.552 955	−0.100 784	2.672 097	−0.478 886
0.692 420	0.095 160	0.212 420	−0.497 576	1.467 964	−0.107 105	2.635 251	−0.398 970
0.648 990	0.102 020	0.248 990	−0.576 771	1.383 920	−0.112 120	2.605 698	−0.336 924
0.606 258	0.107 484	0.286 258	−0.656 045	1.300 758	−0.116 022	2.582 532	−0.289 481
0.564 177	0.111 646	0.324 177	−0.735 444	1.218 386	−0.118 945	2.565 103	−0.254 443
0.522 714	0.114 572	0.362 714	−0.815 028	1.136 706	−0.120 976	2.552 953	−0.230 341
0.481 844	0.116 312	0.401 844	−0.894 867	1.055 621	−0.122 173	2.545 779	−0.216 230
0.441 556	0.116 888	0.441 556	−0.975 037	0.975 037	−0.122 569	2.543 407	−0.211 582

TABLE IV

Periodic orbits, $m_1 = m_3$

$m_1 = m_3$	m_2	$-x_1 = x_3$	$u_1 = u_3$	T	k_1	k_2
0.	1.	1.673 612	−0.441 611	6.283 185	2.	2.
0.02	0.96	1.662 672	−0.427 962	6.261 636	1.692 301	1.998 187
0.06	0.88	1.638 699	−0.400 562	6.204 575	1.068 490	1.981 487
0.10	0.80	1.611 441	−0.373 018	6.124 824	0.441 729	1.941 098
0.14	0.72	1.580 138	−0.345 313	6.016 147	−0.173 882	1.866 262
0.18	0.64	1.543 774	−0.317 425	5.870 221	−0.757 751	1.740 473
0.22	0.56	1.500 955	−0.289 323	5.675 770	−1.280 234	1.537 712
0.26	0.48	1.449 716	−0.260 957	5.417 254	−1.699 229	1.215 886
0.30	0.40	1.387 184	−0.232 242	5.072 851	−1.955 939	0.706 190
0.322 581	0.354 838	1.345 328	−0.215 824	4.829 213	−2.	0.296 891
0.333 333	0.333 334	1.323 348	−0.207 939	4.698 084	−1.988 976	0.062 601
0.34	0.32	1.308 968	−0.203 024	4.611 314	−1.970 496	−0.096 853
0.36	0.28	1.261 914	−0.188 136	4.323 118	−1.855 702	−0.642 774
0.38	0.24	1.207 937	−0.172 973	3.987 051	−1.640 491	−1.272 088
0.40	0.20	1.145 274	−0.157 412	3.593 945	−1.310 396	−1.858 178
0.410 964	0.178 072	1.106 380	−0.148 639	3.350 303	−1.076 066	−2.
0.42	0.16	1.071 437	−0.141 230	3.132 636	−0.853 142	−1.835 164
0.43	0.14	1.029 240	−0.132 783	2.872 269	−0.574 580	−0.992 562
0.44	0.12	0.982 715	−0.123 979	2.589 541	−0.262 950	1.385 346
0.441 556	0.116 888	0.975 037	−0.122 569	2.543 407	−0.211 582	2.
0.45	0.10	0.931 027	−0.114 667	2.282 257	0.080 055	7.425 331
0.46	0.08	0.873 032	−0.104 583	1.947 877	0.450 830	23.121 22
0.47	0.06	0.807 059	−0.093 232	1.583 150	0.842 952	68.981 76
0.48	0.04	0.730 366	−0.079 533	1.182 759	1.245 748	242.581 6
0.49	0.02	0.637 325	−0.060 362	0.732 288	1.641 762	1487.570
0.50	0.	0.5	0.	0.	2.	∞

account the normalization (5), we find that the semi-major axis is 1 and the period is 2π. If t_0 is the time of a 1–2 collision, the motions of bodies 1 and 2 are given in parametric form by

$$x_1 = -m_2(1 - \cos E), \qquad x_2 = m_1(1 - \cos E),$$
$$t = t_0 = E - \sin E. \tag{14}$$

The motion of the third body, on the other hand, is not trivial and can only be obtained from numerical integration. An example of an orbit which is not actually at the limit $m_3 = 0$, but close to it, is shown in Figure 6; it corresponds to $m_1 = 0.504\,353\ldots$, $m_2 = 0.491\,294\ldots$, $m_3 = 0.004\,353\ldots$ (incidentally, this is a critical orbit with $k_1 = -2$).

The results of Section 2 show that orbits with $m_3 = 0$ are stable for $0.492\,82\ldots < m_2 < 1$; unstable longitudinally for $0.1321\ldots < m_2 < 0.492\,82\ldots$; and unstable both longitudinally and transversally for $0 < m_2 < 0.1321\ldots$.

(b) *Limit* $m_2 \to 0$. This case, which corresponds to the bottom side of the triangle, is quite interesting. An example close to the limit is shown on Figure 7, for $m_1 = 0.495$,

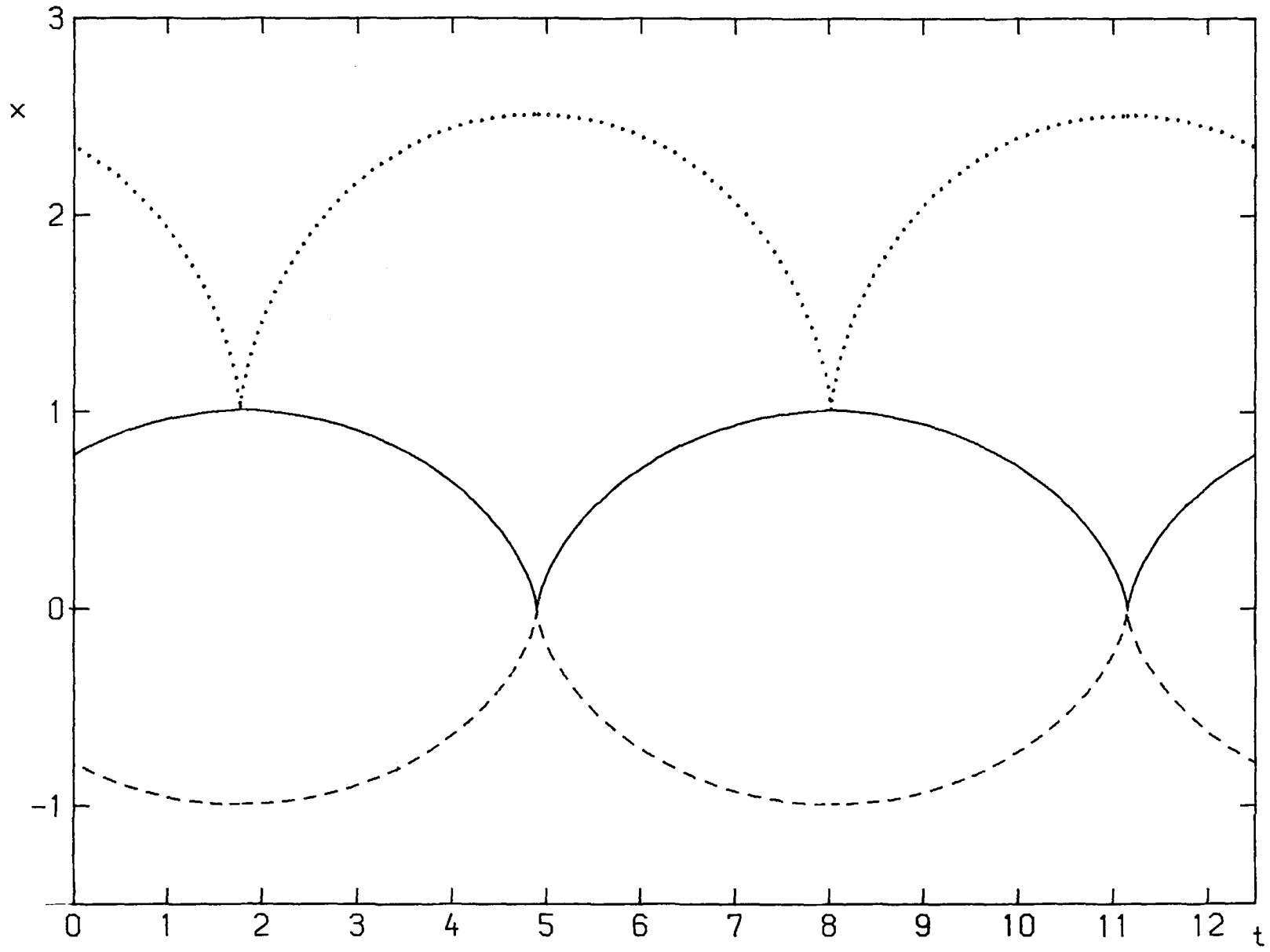

Fig. 6. An orbit close to the limit $m_3 \to 0$.

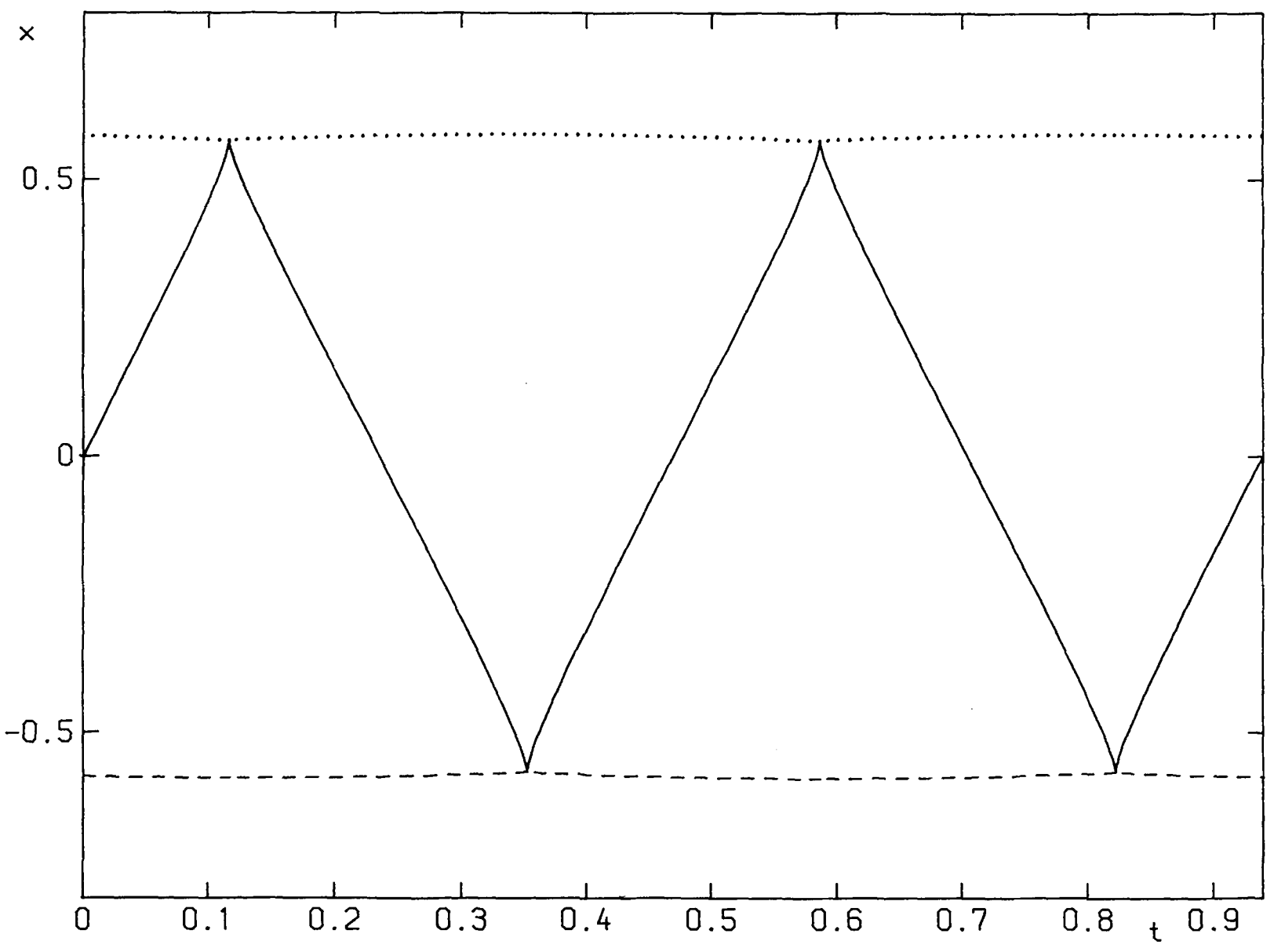

Fig. 7. An orbit close to the limit $m_2 \to 0$.

$m_2 = 0.01$, $m_3 = 0.495$. It can be seen that the central body moves quickly back and forth while bodies 1 and 3 are almost motionless. As m_2 tends to zero, its velocity tends to infinity, and the period tends to zero (see end of Table IV). This is easy to explain: only the repeated collisions with body 2 prevent bodies 1 and 3 from falling

towards the center of the system; therefore, as m_2 decreases, its velocity must increase so as to still transfer a sufficient momentum at each collision.

Asymptotic expressions are easily derived. Since the period is very short, we can neglect the displacement of bodies 1 and 3: x_1 and x_3 are assumed to be constants. Also, since the velocity of body 2 is large, we can take it as constant between collisions. Because of the time symmetry, we have then $u_2 = \pm u$, where u is a constant. The period is

$$T = \frac{2(x_3 - x_1)}{u}. \tag{15}$$

The momentum transferred to body 1 at each collision is $-2m_2u$. The total force exerted on body 1 from the repeated collisions with body 2 and from the attraction of body 3 must vanish:

$$-\frac{2m_2u}{T} + \frac{m_1m_3}{(x_3 - x_1)^2} = 0. \tag{16}$$

Finally, the normalization (5) gives

$$E = \tfrac{1}{2}m_2u^2 - \frac{m_1m_3}{x_3 - x_1} = -\tfrac{1}{2}m_1m_3. \tag{17}$$

From these three equations we obtain

$$x_3 - x_1 = 1, \qquad u = \left(\frac{m_1m_3}{m_2}\right)^{1/2}, \qquad T = 2\left(\frac{m_2}{m_1m_3}\right)^{1/2}. \tag{18}$$

The system can be described as two attracting bodies 1 and 3, separated by a weightless gas whose pressure equilibrates the attractive force; the gas consists of a single molecule m_2!

The present case is unusual because one of the masses tends to zero, yet in the limit we do *not* reach the classical restricted three-body problem: the motion of bodies 1 and 3 does not become a two-body motion. This is because the effect of body 2 does not become negligible in the limit.

Approximate expressions can also be obtained for the stability indices. We consider first the longitudinal stability. Suppose that the equilibrium values (18) are perturbed by small amounts $\Delta(x_3 - x_1)$, Δu, ΔT. Equations (15) and (17) still hold for the perturbed motion and give by differentiation

$$\Delta u = -u\Delta(x_3 - x_1), \qquad \Delta T = \frac{4}{u}\Delta(x_3 - x_1). \tag{19}$$

Equation (16) is no more satisfied by the perturbed motion; its left-hand side gives the force acting on particle 1. Differentiating and substituting (19), we obtain for this force:

$$m_1 \frac{\mathrm{d}^2}{\mathrm{d}t^2}\Delta x_1 = m_1m_3\Delta(x_3 - x_1). \tag{20}$$

Combining this with a similar equation for body 3, we have

$$\frac{d^2}{dt^2}\Delta(x_3 - x_1) = -\Delta(x_3 - x_1) \tag{21}$$

with the general solution

$$\Delta(x_3 - x_1) = C_1 e^{it} + C_2 e^{-it}. \tag{22}$$

The perturbation oscillates with period 2π: the motion is longitudinally stable. This oscillation is superimposed on the much shorter period T of the motion itself. Equation (22) shows that the eigenvalues are $e^{\pm iT}$ and their sum, i.e., the longitudinal stability index, is

$$k_1 = 2\cos T \tag{23}$$

or, using (18):

$$k_1 \approx 2 - \frac{4m_2}{m_1 m_3}. \tag{24}$$

This expression is in good agreement with the numerical results for $m_2 \to 0$ (see Figures 3 and 4 and the last lines of Table IV).

Next we consider the transversal stability. We again assume that m_1 and m_3 are motionless, and that m_2 has a constant velocity u between collisions. In a transversally perturbed orbit, the motion of body 2 lies no more on the x axis, and collisions are replaced by close approaches, with body 2 describing near-parabolic hairpin turns around bodies 1 and 3 in alternance. Let l be the impact parameter at one close approach of m_3 by m_2. The deflection angle is given by the classical formula

$$\tan\frac{\beta}{2} = \frac{m_3}{u^2 l}. \tag{25}$$

β is not quite equal to π, so that body 2 does not come back straight at body 1, but deviates by a small angle $\pi - \beta$. Therefore the impact parameter at the next close approach of body 1 is

$$l' = (x_3 - x_1)\sin(\pi - \beta) \tag{26}$$

or, using (18) and (25):

$$l' \approx \frac{2m_1}{m_2} l. \tag{27}$$

Similarly, the next close approach of body 3 will have an impact parameter

$$l'' = \frac{2m_3}{m_2} l' \tag{28}$$

and the net amplification factor after one period is

$$\frac{l''}{l} = \frac{4m_1m_3}{m_2^2}. \tag{29}$$

For m_2 small, this is a large quantity: the orbit is strongly unstable transversally. One eigenvalue is equal to (29), while the other is its inverse and is very small. Thus the transversal stability index is

$$k_2 \approx \frac{4m_1m_3}{m_2^2}. \tag{30}$$

This asymptotic expression is in reasonable agreement with the numerical results (see end of Table IV). For $m_2 \to 0$, we have $k_2 \to +\infty$. This explains why the bottom of the triangle in Figure 5 is entirely occupied by a region of transversally unstable orbits.

(c) *Limit* $m_2 \to 0$, $m_3 \to 0$. This case corresponds to the left vertex of the triangle. An example is shown on Figure 8 for $m_1 = 0.973\,090\ldots$, $m_2 = 0.013\,820\ldots$, $m_3 = 0.013\,090\ldots$ (second line of Table I). Body 1, having all the mass, is motionless at the origin: $x_1 = 0$. Bodies 2 and 3 have no effect upon each other between collisions and describe independent two-body orbits in the field of body 1; the collisions themselves are like billiard-ball collisions. The parameters of the orbit can then be derived as follows. Let t_0 be again the time of a 1–2 collision. Two cases must be distinguished, depending on whether the motion of body 2 is elliptic or hyperbolic. In the first case, it is given in parametric form between the times $t_0 - T/2$ and $t_0 + T/2$ by

$$x_2 = a_2(1 - \cos E_2), \qquad t - t_0 = a_2^{3/2}(E_2 - \sin E_2),$$
$$u_2 = a_2^{-1/2}\frac{\sin E_2}{1 - \cos E_2}, \tag{31}$$

where the semi-major axis a_2 is a constant to be determined and the eccentric anomaly E_2 is the parameter. The motion of body 3 is always elliptical, and is similarly given between times $t_0 - T/2$ and $t_0 + T/2$ by

$$x_3 = a_3(1 + \cos E_3), \qquad t - t_0 = a_3^{3/2}(E_3 + \sin E_3),$$
$$u_3 = -a_3^{-1/2}\frac{\sin E_3}{1 + \cos E_3}. \tag{32}$$

At $t = t_0 + T/2$, bodies 2 and 3 collide and there must be

$$x_2 = x_3, \qquad m_2u_2 = -m_3u_3, \tag{33}$$

the last equation expressing the conservation of momentum during the collision. Finally, the normalization (5) of the energy gives

$$-\tfrac{1}{2}\left(\frac{m_2}{a_2} + \frac{m_3}{a_3}\right) = -\tfrac{1}{2}(m_2 + m_3). \tag{34}$$

From Equations (31) to (34) one deduces

$$\frac{(1-\cos E_2)^3}{(E_2-\sin E_2)^2}=\frac{(1+\cos E_3)^3}{(E_3+\sin E_3)^2}, \tag{35}$$

$$\frac{m_3}{m_2}=\left(\frac{1+\cos E_3}{1-\cos E_2}\right)^{1/2}\frac{\sin E_2}{\sin E_3}, \tag{36}$$

where E_2 and E_3 represent now the values at the time of collision. For a given ratio m_3/m_2, Equations (35) and (36) constitute a set of two implicit equations for E_2 and E_3, which must be solved numerically. The semi-major axes are then given by

$$a_2=\frac{(1-\cos E_2)+\dfrac{m_3}{m_2}(1+\cos E_3)}{\left(1+\dfrac{m_3}{m_2}\right)(1-\cos E_2)},$$

$$a_3=\frac{(1-\cos E_2)+\dfrac{m_3}{m_2}(1+\cos E_3)}{\left(1+\dfrac{m_3}{m_2}\right)(1+\cos E_3)}. \tag{37}$$

If the motion of body 2 is hyperbolic, (31) must be replaced by

$$x_2=-a_2(\cosh F_2-1), \qquad t-t_0=(-a_2)^{3/2}(\sinh F_2-F_2),$$

$$u_2=(-a_2)^{-1/2}\frac{\sinh F_2}{\cosh F_2-1}, \tag{38}$$

with $a_2<0$. Equations (32) to (34) still hold. Equations (35) to (37) are replaced by

$$\frac{(\cosh F_2-1)^3}{(\sinh F_2-F_2)^2}=\frac{(1+\cos E_3)^3}{(E_3+\sin E_3)^2}, \tag{39}$$

$$\frac{m_3}{m_2}=\left(\frac{1+\cos E_3}{\cosh F_2-1}\right)^{1/2}\frac{\sinh F_2}{\sin E_3}, \tag{40}$$

$$a_2=-\frac{\dfrac{m_3}{m_2}(1+\cos E_3)-(\cosh F_2-1)}{\left(1+\dfrac{m_3}{m_2}\right)(\cosh F_2-1)},$$

$$a_3=\frac{\dfrac{m_3}{m_2}(1+\cos E_3)-(\cosh F_2-1)}{\left(1+\dfrac{m_3}{m_2}\right)(1+\cos E_3)}. \tag{41}$$

Table V gives some numerical values. The second column gives E_2 if $a_2>0$, F_2 if $a_2<0$. The column X gives the common abscissa of bodies 2 and 3 when they collide.

TABLE V

Periodic orbits in the limit $m_2 \to 0$, $m_3 \to 0$

m_3/m_2	E_2 or F_2	E_3	a_2	a_3	T	X	k_1
0.	3.141 593	1.086 255	1.	1.364 440	6.283 185	2.	−10.103 776
0.1	3.041 428	1.048 620	0.977 388	1.300 987	5.684 456	1.949 877	−8.291 318
0.2	2.946 893	1.014 967	0.961 851	1.247 362	5.194 752	1.905 530	−6.901 149
0.4	2.771 101	0.957 051	0.947 325	1.161 453	4.442 426	1.830 373	−4.929 177
0.6	2.608 660	0.908 689	0.950 329	1.095 424	3.892 103	1.768 868	−3.614 386
0.8	2.455 825	0.867 454	0.968 140	1.042 900	3.472 311	1.717 416	−2.685 569
1.	2.309 881	0.831 711	1.	1.	3.141 593	1.673 612	−2.
1.2	2.168 729	0.800 312	1.046 607	0.964 218	2.874 299	1.635 779	−1.476 290
1.5	1.962 225	0.759 595	1.149 231	0.920 329	2.557 287	1.587 673	−0.891 238
2.	1.619 130	0.704 279	1.453 912	0.864 977	2.174 891	1.524 157	−0.239 314
3.	0.804 578	0.623 495	4.682 320	0.792 303	1.702 973	1.435 528	0.479 759
3.388 734	0.	0.599 111	∞	0.772 144	1.578 208	1.409 809	0.653 145
5.	1.492 946	0.522 645	−0.996 308	0.713 908	1.232 727	1.332 510	1.093 851
10.	2.606 877	0.397 974	−0.209 533	0.634 014	0.793 121	1.218 479	1.560 856
20.	3.480 886	0.294 832	−0.074 511	0.581 045	0.518 568	1.137 018	1.787 513
∞	∞	0.	0.	0.5	0.	1.	2.

Note that for $m_3/m_2 \to 0$, we recover case (a) above, while for $m_3/m_2 \to \infty$ we recover case (b).

The longitudinal stability can be computed as follows. Consider a perturbed orbit, in which the changes in the position and time of a collision 2–3 are ΔX and $\Delta\tau$, while the changes in the velocities just after the collision are Δu_2 and Δu_3. From this one deduces successively the perturbations in the orbital elements of bodies 2 and 3; the perturbations $\Delta' X$ and $\Delta'\tau$ in the position and time of the next collision; the perturbations of the velocities just before that collision; and finally the perturbations $\Delta' u_2$ and $\Delta' u_3$ of the velocities just after it. The computations are tedious and will not be reproduced here. The result is a matrix $\mathbf{M}$ such that

$$\begin{pmatrix} \Delta' X \\ \Delta'\tau \\ \Delta' u_2 \\ \Delta' u_3 \end{pmatrix} = \mathbf{M} \begin{pmatrix} \Delta X \\ \Delta\tau \\ \Delta u_2 \\ \Delta u_3 \end{pmatrix}. \tag{42}$$

Two of the eigenvalues of $\mathbf{M}$ are equal to 1; they correspond respectively to a shift in time and to a change of scale of the orbit. The two other eigenvalues give the longitudinal stability. Thus, the trace of $\mathbf{M}$ is equal to $2+k_1$, and one obtains

$$k_1 = 2 + \frac{12 \sin E_3 (E_3 + \sin E_3)}{(1 + \cos E_3)^3} \left(\frac{m_3}{m_2} - 1\right) a_2 - 4 a_2 a_3 . \tag{43}$$

Numerical values are given in Table V. The orbits are longitudinally stable for

$m_3 > m_2$, unstable for $m_3 < m_2$. For $m_2 = m_3$, k_1 equals -2 exactly. This peculiarity can be explained as follows. For $m_2 = m_3$, the velocities of bodies 2 and 3 are simply exchanged during a collision. Suppose that after each collision we exchange the identities of 2 and 3. Then the two bodies pass through each other without any interaction, and describe for all times independent two-body motions. The period of these motions is $2T$, as can be seen on Figure 8. Consider now a perturbed orbit in which one of the motions is shifted in time by an amount $+\Delta\tau$, and the other is shifted by an amount $-\Delta\tau$. The periods do not change. If now we reestablish the original identities, we find that after each period T the shifts of bodies 2 and 3 change sign. This corresponds to an eigenvalue -1. The last eigenvalue must then be also -1, and $k_1 = -2$.

As a consequence, the boundary line $k_1 = -2$ on Figure 5 ends in the vertex 1 with a slope corresponding to $m_2 = m_3$, i.e., it is tangent to the bisectrix of the angle.

To determine the transversal stability, we consider a perturbed orbit in which small motions in the y direction are superimposed on the rectilinear motion. Bodies 2 and 3 describe then elongated ellipses around body 1. Suppose that they have just had a collision. In the general case $m_2 \neq m_3$, the two bodies will describe different orbits and they will 'miss' each other at the next period. Thereafter the perturbed motion becomes entirely different from the unperturbed motion. This corresponds to an infinite eigenvalue: therefore $k_2 = \pm\infty$ in general.

In the particular case $m_2 = m_3$, however, there is $v_2 = -v_3$ after a collision since the total angular momentum must be zero in the perturbed orbit also (see Hénon, 1976).

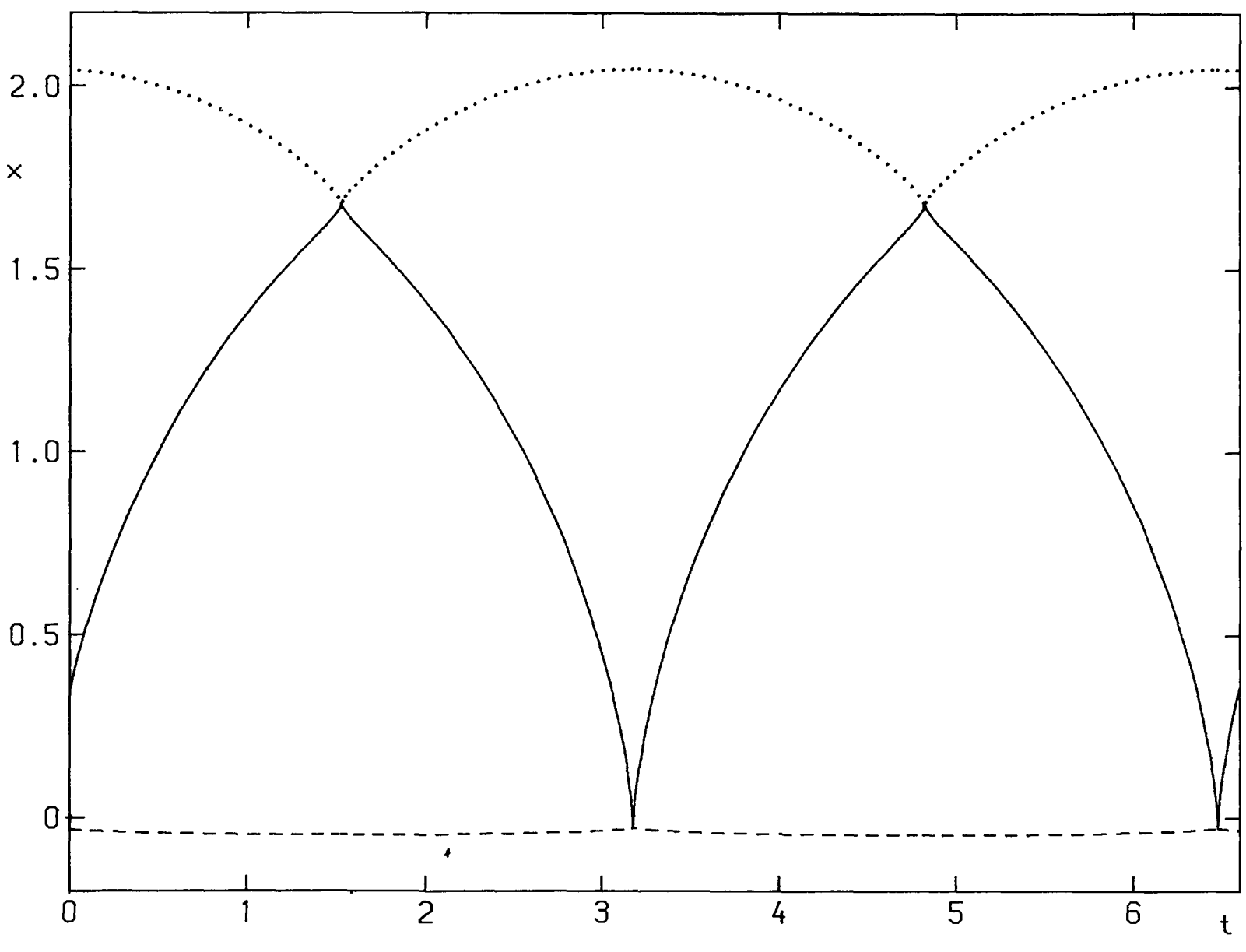

Fig. 8. An orbit close to the limit $m_2 \to 0$, $m_3 \to 0$.

There is also $u_2 = -u_3$ since these values are the same as in the unperturbed motion. Therefore the two bodies describe the same orbit in opposite directions, and they will collide again.

If we make the ratio m_3/m_2 change continuously, the transversal stability index will jump from $-\infty$ to $+\infty$ when m_3/m_2 crosses the value 1. Numerical results confirm this, and indicate that $k_2 = +\infty$ for $m_3 > m_2$, $k_2 = -\infty$ for $m_3 < m_2$. We remark also that when jumping from $-\infty$ to $+\infty$, k_2 passes through the values -2 and $+2$. This explains why the boundary curves $k_2 = -2$ and $k_2 = +2$ also end in vertex 1 tangentially to the bisectrix $m_2 = m_3$ (Figure 5).

(d) *Limit* $m_1 \to 0$, $m_3 \to 0$. This case corresponds to the top vertex of the triangle. An example is given in Figure 9 for $m_1 = 0.001$, $m_2 = 0.998$, $m_3 = 0.001$. Here the motion is quite simple. Body 2, having all the mass, sits motionless at the origin. There is no interaction between bodies 1 and 3 since they are on opposite sides of the massive body 2, and they describe independent elliptical two-body orbits with eccentricity 1. Their periods must be the same and therefore their semi-major axes are equal. From the condition (5) one finds then that the semi-major axes equal 1, and the period is 2π. The motions of the three bodies are in parametric form:

$$\begin{aligned} x_1 &= -(1 - \cos E_1), \qquad t - t_0 = E_1 - \sin E_1; \\ x_2 &= 0; \\ x_3 &= 1 - \cos E_3, \qquad t - t_0 - \pi = E_3 - \sin E_3. \end{aligned} \tag{44}$$

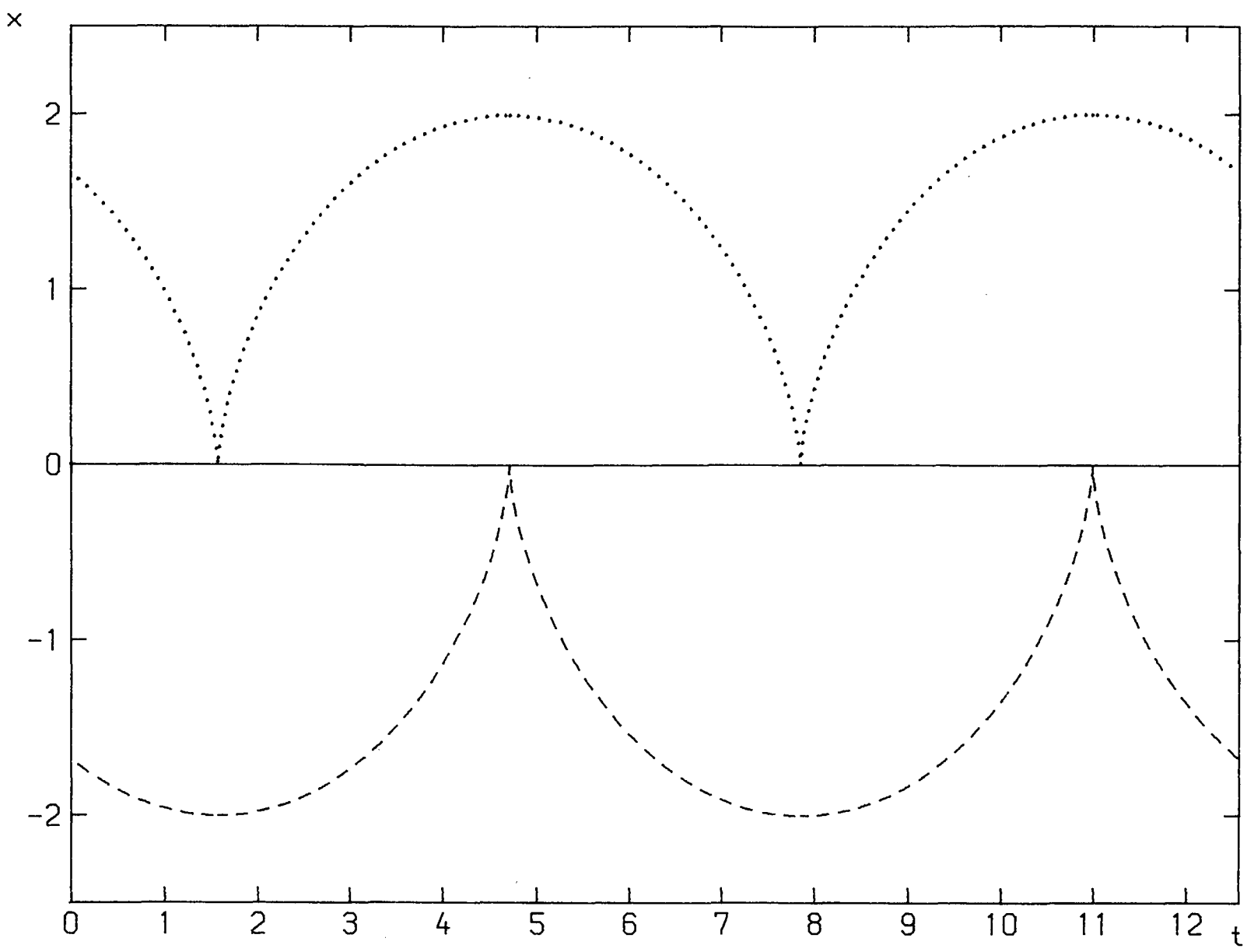

Fig. 9. An orbit close to the limit $m_1 \to 0$, $m_3 \to 0$.

Note that this limiting orbit is independent of the ratio m_3/m_1, in contrast to the situation in the previous case (c).

Since we have a superposition of two independent two-body motions with the same period, all eigenvalues are equal to 1, and

$$k_1 = +2, \qquad k_2 = +2. \tag{45}$$

This is confirmed by the numerical results (Figure 4).

References

Hénon, M.: 1973, *Astron. Astrophys.* **28**, 415.
Hénon, M.: 1974, *Celes. Mech.* **10**, 375.
Hénon, M.: 1976, *Celes. Mech.* **13**, 267.
Schubart, J.: 1956, *Astron. Nachr.* **283**, 17.
Standish, E. M.: 1972, *Astron. Astrophys.* **21**, 185.
Szebehely, V.: 1971, *Celes. Mech.* **4**, 116.
Szebehely, V.: 1972, *Proc. Nat. Acad. Sci. U.S.A.* **69**, 1077.
Waldvogel, J.: 1972, *Celes. Mech.* **6**, 221.